Mon. Not. R. Astron. Soc. **270,** 947–957 (1994)

The UK Deep and Medium Surveys with *ROSAT*: log *N*–log *S* relation

G. Branduardi-Raymont,[1] K. O. Mason,[1] R. S. Warwick,[2] F. J. Carrera,[1] V. G. Graffagnino,[1] J. P. D. Mittaz,[1] E. M. Puchnarewicz,[1] P. J. Smith,[1] C. R. Barber,[2] K. A. Pounds,[2] G. C. Stewart,[2] I. M. McHardy,[3] L. R. Jones,[3] M. R. Merrifield,[3] A. C. Fabian,[4] R. G. McMahon,[4] M. J. Ward,[5] I. M. George,[6]★ M. H. Jones,[7] A. Lawrence[8] and M. Rowan-Robinson[9]

[1] *Mullard Space Science Laboratory, University College London, Holmbury St Mary, Dorking, Surrey RH5 6NT*
[2] *X-ray Astronomy Group, Physics Department, University of Leicester, Leicester LE1 7RH*
[3] *Physics Department, University of Southampton, Highfield, Southampton SO9 5NH*
[4] *Institute of Astronomy, Madingley Road, Cambridge CB3 0HA*
[5] *Department of Astrophysics, University of Oxford, South Parks Road, Oxford OX1 3RQ*
[6] *Code 668, NASA/Goddard Space Flight Center, Greenbelt, Md 20771, USA*
[7] *Academic Computer Services, The Open University, Walton Hall, Milton Keynes MK7 6AA*
[8] *Department of Physics, Queen Mary and Westfield College, Mile End Road, London E1 4NS*
[9] *Department of Physics, Blackett Laboratory, Imperial College of Science, Technology and Medicine, Prince Consort Road, London SW7 2BZ*

Accepted 1994 June 24. Received 1994 June 21; in original form 1992 December 21

ABSTRACT

We have carried out a soft X-ray survey of the sky using the *ROSAT* Position Sensitive Proportional Counter (PSPC) in a region of very low Galactic column density ($N_H = 6–9 \times 10^{19}$ cm^{-2}). The data consist of a deep >70 ks pointing (the Deep Survey) and six pointings at lower sensitivity (13–20 ks; the Medium Survey). We detect a total of 141 sources over the 0.9 deg^2 of sky area used. The faintest source detected has a flux of 3.2×10^{-15} erg cm^{-2} s^{-1} (0.5–2.0 keV). We present the source number–flux distribution, and we compare it with the distributions constructed from other *ROSAT* observations and from surveys carried out with X-ray instruments operating at higher energies. We estimate the contribution of the resolved sources to the soft X-ray background by direct comparison of their integrated spectrum with that of the diffuse background: 44 per cent of the extragalactic X-ray background between 0.5 and 2.0 keV is resolved directly into discrete sources whose average spectrum is steeper than that of the background. Integration of our number–flux relation to infinite flux produces a background resolved fraction of $44 \pm ^{56}_{5}$ per cent (0.5–2.0 keV). Limits on the slope of the log *N*–log *S* curve at very faint fluxes are set by the measured value of the X-ray background.

Key words: galaxies: active – diffuse radiation – X-rays: general.

1 INTRODUCTION

The *ROSAT* X-ray Telescope provides images of unparalleled sensitivity in the soft X-ray spectral band, between 0.1 and 2.5 keV. To exploit this sensitivity we have conducted a >70-ks-long observation in a region of sky that has very low Galactic absorption (6.5×10^{19} cm^{-2}), with the aim of exploring the population of faint X-ray sources, most of which are expected to be extragalactic. We refer to this as the UK Deep Survey. To complement the Deep Survey and to improve the statistics on intermediate brightness sources in our sample, we have made a series of six 13- to 20-ks-long observations, the Medium Survey, also in a region of low Galactic obscuration ($\sim 8 \times 10^{19}$ cm^{-2}) and spanning a 6 deg^2 area of sky.

Deep X-ray surveys have a central role to play in understanding the population and evolutionary characteristics of faint extragalactic sources, and the contribution of such sources to the X-ray 'background' flux. In this paper we combine the data from the Deep and Medium Surveys to

★ Also at Universities Space Research Association.

investigate the number–flux distribution of soft X-ray sources down to a flux level of 3.2×10^{-15} erg cm^{-2} s^{-1} (0.5–2.0 keV) i.e. one order of magnitude fainter than possible with, for example, the *Einstein Observatory* Deep Survey (Hamilton, Helfand & Wu 1991; Primini et al. 1991). At this flux level we expect to be in a regime where the number–flux relation is turning over from a Euclidean distribution, which it has to do if the integrated flux from the point source population is not to exceed the measured level of the X-ray background radiation.

We present the observations and their analysis in Section 2, we derive the cumulative number–flux (log N–log S) distribution in Section 3, and we determine the contribution of the sources to the diffuse soft X-ray background in Section 4. In Section 5 we compare the log N–log S relation in the Deep and Medium Surveys with those obtained from other surveys and we discuss the implications of our results. Our conclusions are in Section 6.

2 OBSERVATIONS AND POINT SOURCE ANALYSIS

2.1 Low-energy absorption

Soft X-ray observations are severely affected by the absorption caused by the interstellar medium in our own Galaxy. A low equivalent column density of neutral hydrogen in the line of sight is thus an important prerequisite for a soft X-ray survey, because it improves the chance of detecting faint sources, and more importantly removes any potential biases caused by variations in the absorbing column across the survey field. For this reason we have carried out the Deep and Medium Surveys in two of the Lockman 'holes' (L3 and L7, respectively; Lockman, Jahoda & McCammon 1986). These are among the regions of sky with the lowest column densities of neutral hydrogen ($N_{\rm H}\sim8\times10^{19}$ cm^{-2}) listed in the Stark et al. (1992) catalogue.

Maps of the *IRAS* 100-μm cirrus emission have been shown to correlate well with the H I emission (Boulanger & Pérault 1988; Rowan-Robinson et al. 1991). Thus we can use the *IRAS* cirrus measurements to probe the Galactic absorption on smaller angular scales, 1 arcmin, than the Lockman et al. measurements, which had an angular resolution of 20 arcmin. The *IRAS* data in the region of interest are first binned on a similar scale ($\sim2°$) to the Stark et al. radio 21-cm data, and a 'local' relation between the 21-cm and 100-μm data is derived. This is then applied to the *IRAS* data at full resolution to estimate the equivalent hydrogen absorbing column.

The results suggest that the absorbing column over the Deep Survey area is very uniform, with fluctuations of $\sim2\times10^{19}$ cm^{-2} on a mean column of 6.5×10^{19} cm^{-2}. The region covered by the Medium Survey is less uniform, with a mean column of 7.9×10^{19} cm^{-2} and fluctuations of $\sim4\times10^{19}$ cm^{-2} (Jones et al. 1994). We have also obtained 21-cm maps of our *ROSAT* survey regions with the Lovell telescope at Jodrell Bank, at 12-arcmin angular resolution. These confirm the 100-μm results and, in particular, the very uniform absorbing column in the Deep Survey area (Jones et al. 1994).

A log of the *ROSAT* PSPC observations of the Deep Survey region and of the six Medium Survey fields is contained in Table 1. The mean hydrogen column density in each survey field, as inferred from the *IRAS* measurements, is also listed in the Table.

2.2 Source search

Fig. 1 is a grey-scale image (smoothed with a two-dimensional Gaussian of 30-arcsec FWHM) of the inner 20-arcmin radius of the Deep Survey field in the 0.4–2.5 keV band. Several sources can be distinguished by eye above the background level. The sources in the outer part of the image are clearly more extended than in the centre, reflecting the fact that the point spread function (PSF) widens with off-axis angle. To avoid possible biases in source detection caused by the change in PSF, we have restricted the analysis to the inner 12-arcmin radius of all survey fields, where the PSF can be considered constant. We have also rejected data intervals with high anticoincidence rate (Master Veto Rate > 170) or bad aspect ratio. This has left 69.5 ks of 'clean' data.

A point source search was carried out on the 0.4–2.5 keV images, rather than on the full operational band of the PSPC (0.1–2.5 keV). We chose this restricted energy range because

Table 1. Log of the *ROSAT* Deep and Medium Survey observations.

Field	Date (Year/Day no.)	*RA* (2000) h	m	s	*DEC* (2000) °	′	″	Exposure time (s)	N_H (cm^{-2})	Number of detections (0.4 – 2.5 keV)	Min. flux detected (0.5 – 2.0 keV, erg cm^{-2} s^{-1})	Signal-to-Noise Ratio (*SNR*)	*SNR* = 5 flux limit (0.5 – 2.0 keV, erg cm^{-2} s^{-1})
Deep Survey	91/174–177	13	34	37.0	+37	54	44	73311	6.5×10^{19}	47	$(3.2\pm1.0)\times10^{-15}$	4.0	4.7×10^{-15}
Med. Sur. 1	92/132–136	10	10	18.1	+54	45	14	13375	7.7×10^{19}	11	$(11.9\pm4.1)\times10^{-15}$	3.6	2.2×10^{-14}
Med. Sur. 2	91/103–104	10	10	16.5	+53	45	14	14232	8.2×10^{19}	21	$(10.3\pm3.5)\times10^{-15}$	3.5	2.0×10^{-14}
Med. Sur. 3	91/104,115,125–127, 129–130	10	10	15.0	+52	45	14	13358	6.7×10^{19}	18	$(9.0\pm3.4)\times10^{-15}$	3.2	2.1×10^{-14}
Med. Sur. 4	91/106–107,111,114, 129,321,322,324	10	10	13.5	+51	45	14	20178	6.7×10^{19}	13	$(8.3\pm2.8)\times10^{-15}$	3.7	1.5×10^{-14}
Med. Sur. 5	91/316–317	10	10	12.1	+50	45	14	13583	8.7×10^{19}	14	$(10.4\pm3.8)\times10^{-15}$	3.4	2.1×10^{-14}
Med. Sur. 6	91/132–136	10	10	19.8	+55	45	14	18238	9.1×10^{19}	17	$(8.2\pm3.0)\times10^{-15}$	3.5	1.6×10^{-14}

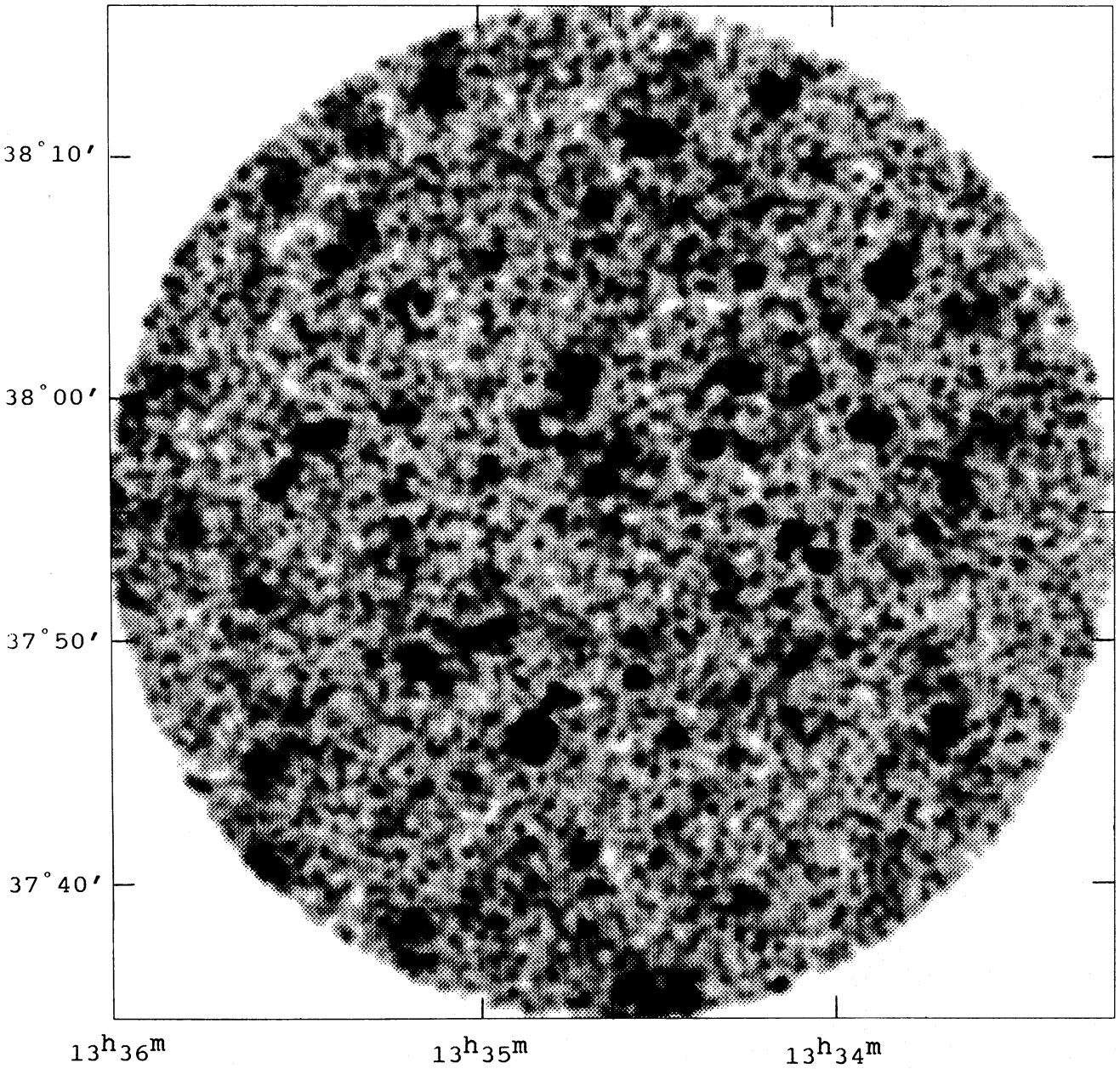

Figure 1. Grey-scale image of the inner 20-arcmin radius of the Deep Survey field (0.4–2.5 keV), smoothed with a two-dimensional Gaussian of 30-arcsec FWHM.

it maximizes the sensitivity to point sources: the PSPC internal background is lowest in the hard X-ray band, and contamination by the Galactic component of the diffuse soft X-ray background, and by solar X-rays scattered in the Earth's atmosphere, is less severe (Snowden et al. 1992). Moreover, the effects of Galactic absorption, although small in the fields under study (see Table 1), are further minimized by excluding the very soft band (0.1–0.4 keV).

The data were analysed with the UK ASTERIX software system and a point source search algorithm (PSS), which uses the Cash (1979) maximum likelihood statistic to determine how well a flux enhancement in the image matches the instrument PSF (Allan & Ponman 1991). In practice, the spatial distribution of counts around each pixel in the image is compared with a model comprising a background level and the PSF, and the Cash statistic is used to define confidence regions for the flux and position of each candidate source. Those candidate sources whose positive flux exceeds a set probability threshold are regarded as real sources.

The level of the background in the survey images was determined in the following way. First, we plotted the radial distribution of the total counts in the images. The level of counts in a source-free annulus was noted and this was used as the background level in a preliminary run of PSS. The sources detected in this first pass were then masked out and the radial distribution plot constructed again: this shows that the background is constant within a few per cent out to 12 arcmin off-axis (for the Deep Survey field we measure it at

0.12 count pixel^{-1}, using pixels of size 4.5 arcsec). Finally, PSS was run again on the original images, adopting the revised, constant background value.

We have used a PSF developed from the energy-dependent model fits of Hasinger et al. (1992). We have weighted their 'monochromatic' PSFs by the relative number of PSPC counts expected for a power-law spectrum of energy index $\alpha = 1.1$ (consistent, within the errors, with the slope of the average source spectrum in our Deep Survey; see Section 4), and a hydrogen column density equal to that measured for each field. We have checked the validity of our technique on bright sources observed by the PSPC nearly on-axis. We find that adoption of the spectrum-weighted PSF leads to fluxes 20 per cent higher than those obtained using the default ASTERIX PSF (a Gaussian with 24-arcsec FWHM). Although the latter is a good representation of the core of the PSF, the spectrum-weighted PSF is preferred here because it provides a more accurate measure of the PSF wings than the default ASTERIX or the 'monochromatic' PSFs.

The PSF fit was carried out over a region of 18-arcsec radius, which encircles about 60 per cent of the energy in a point source image, using pixels of size 4.5 arcsec. Although only the core of the PSF was fitted in this way, source fluxes were estimated by integrating the whole PSF, including its wings in full.

We set the probability threshold for a source to be real at more than 99.99 per cent. This reflects the probability of having a spurious source at that position, rather than anywhere in the field. Assessing the latter is hard to do, especially for the Deep Survey field, where we could expect a population of unresolved sources, skewing the upper tail of the counts distribution and increasing the spurious source detection rate (D. J. Allan, private communication). In practice, we have obtained a measure of the PSS reliability by means of simulations (see Section 3.2).

We detect 47 sources in the Deep Survey field within 12 arcmin of the centre, and a total of 94 sources in the six Medium Survey fields. All sources include at least 9 counts, so the Cash (1979) statistic can be applied with confidence.

The source strengths estimated directly from the PSF fits, in the way described above, were corrected for dead time, vignetting and obscuration by the PSPC window support wires. Finally, source count rates were calculated by dividing by the exposure time appropriate to each field.

To convert from PSPC source count rates to energy fluxes, we need to assume a spectral shape. We have taken a power law of energy index = 1.1 as the source average spectrum (Section 4), and we have corrected the observed fluxes for Galactic absorption, adopting an average value $N_{\rm H} = 8 \times 10^{19}$ cm^{-2} (Table 1). The conversion factor from *ROSAT* PSPC counts (0.4–2.5 keV) to energy flux is then 1 PSPC count s$^{-1} \equiv 1.1 \times 10^{-11}$ erg cm^{-2} s^{-1} (0.5–2.0 keV).

Varying the energy index by ± 0.1 implies only a 0.5 per cent difference in the conversion factor. The minimum flux detected in each field and the corresponding source signal-to-noise ratio (SNR, i.e. the ratio of the source counts to the square root of source plus background counts; see Schmitt & Maccacaro 1986) are listed in Table 1. The minimum fluxes are lower than those expected by requiring a SNR equal to 5 (also listed in Table 1): this condition addresses the accuracy of the flux measurement, rather than the confidence in the source reality, and is sometimes referred to as a '5σ' criterion (e.g. Schmitt & Maccacaro 1986, and references therein). A SNR = 5 approach was taken for the *Einstein Observatory* Medium Sensitivity Survey (MSS) by Maccacaro et al. (1982) and Gioia et al. (1984), and has been shown to lead to an essentially bias-free evaluation of the sources' number–flux distribution (Schmitt & Maccacaro 1986). In our analysis, the requirement imposed by PSS, that the spatial distribution of counts match the PSF distribution, allows us to go deeper than the SNR = 5 limit, while still avoiding serious biases, as our simulations demonstrate (see Section 3.2). Moreover, Maccacaro, Romaine & Schmitt (1987) have pointed out that only a very small number of spurious detections (statistical fluctuations exceeding the detection threshold; Eddington 1940) is expected above SNR = 3, because of the Poissonian nature of the X-ray flux error distribution; all our survey fields satisfy this condition (see Table 1).

Detailed analysis of the spectral and variability characteristics of the sources detected in our survey fields is reserved for a future publication.

3 THE LOG *N*–LOG *S* RELATION

The flux distributions of the sources detected in the Deep and Medium Survey fields are shown in Fig. 2 as histograms. The Deep Survey detections cover the flux range 3.2×10^{-15}–5.6×10^{-13} erg cm^{-2} s^{-1}, while the range seen in the Medium Survey is 8.2×10^{-15}–4.3×10^{-13} erg cm^{-2} s^{-1}.

The brightest source detected (5.6×10^{-13} erg cm^{-2} s^{-1}) is in the field of the Deep Survey (see Fig. 1), where we would expect only 0.03 sources at and above this flux, using the best-fitting log N–log S relation (Gioia, private communication) to the total (Galactic and extragalactic) *Einstein Observatory* Extended Medium Sensitivity Survey (EMSS; see Gioia et al. 1990; Stocke et al. 1991). Moreover, its optical counterpart is a Galactic star, while we are primarily interested in the extragalactic population of our sample. Thus, in constructing the log N–log S relation, we have ignored this source, which would have unrealistically distorted the distribution.

3.1 Fit to the source counts distribution

Following the work of Hasinger et al. (1993, hereafter H93), who have carried out a *ROSAT* survey similar to ours, we have used a broken power law to model the source differential distribution obtained by combining the Deep and Medium Survey data over the range 3.2×10^{-15}–4.3×10^{-13} erg cm^{-2} s^{-1}.

First, we have corrected the data for sky coverage. We take it to be 0.13 deg^2 for fluxes between 3 and 8×10^{-15} erg cm^{-2} s^{-1} (Deep Survey) and 0.88 deg^2 above 8×10^{-15} erg cm^{-2} s^{-1} (Medium and Deep Survey areas combined; see also Section 3.3). This assumes that the same sensitivity limit applies to all the Medium Survey fields, despite their different exposures (Table 1), and simplifies the simulations in Section 3.2 considerably. Use of the sensitivity limits appropriate to each field does not alter our results.

The broken power-law distribution can be represented as follows:

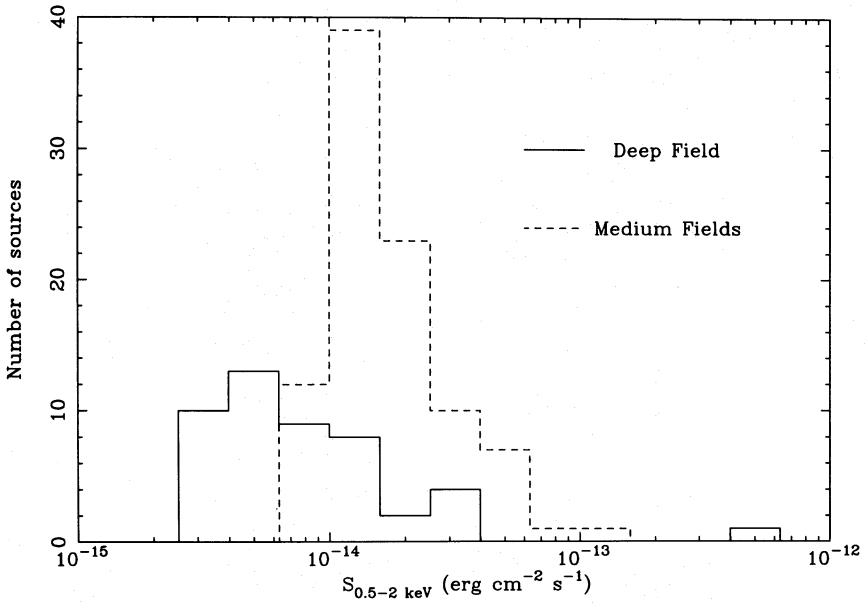

Figure 2. Flux distributions of the sources detected in the Deep (solid line) and Medium (dashed line) Survey fields.

$$n(S)=\frac{K}{S_B}\left(\frac{S}{S_B}\right)^{-\gamma_1} \qquad \text{for } S_{min}<S<S_B,$$

$$n(S)=\frac{K}{S_B}\left(\frac{S}{S_B}\right)^{-\gamma_2} \qquad \text{for } S_B<S<\infty,$$

where S_B is the break flux, $S_{min}=3.2\times10^{-15}$ erg cm^{-2} s^{-1} is the minimum detected flux, and K is the normalization. Initially, we used a maximum likelihood (ML) technique to determine the best-fitting values of the two slopes, γ_1 and γ_2, and the break flux S_B. The normalization K was determined by comparison of the observed number of sources with that predicted by the ML fit. We obtained best-fitting parameters $\gamma_1=1.7$, $\gamma_2=2.7$, $S_B=1.6\times10^{-14}$ erg cm^{-2} s^{-1}; we also found the number of sources per deg^2 at or above 10^{-14} erg cm^{-2} s^{-1}, $N(>10^{-14})=103$.

The sources' cumulative number–flux relation (log N–log S) can be easily derived from their differential distribution. The log N–log S relations constructed separately for the sources in the Deep and Medium Surveys are found to be in good agreement over the flux range covered by both sets of data ($>8\times10^{-15}$ erg cm^{-2} s^{-1}).

3.2 Monte Carlo simulations

We have considered carefully the extent to which the Deep and Medium Survey samples are complete. Source confusion is not expected to be a serious problem in the Medium Survey case: taking the 90 per cent power radius of 27 arcsec as the 'beam' (after convolving the PSF with the pixel size of 4.5 arcsec), and the total number of detections (94), we find one source per 45 beams over the 0.75 deg^2 of the survey; in radio astronomy one source per 40 beams is the limit at which confusion starts becoming a problem (Condon 1974). Confusion is potentially important, however, in the case of the Deep Survey (one source per 15 beams).

To check the completeness and accuracy of our surveys, we have simulated 100 Deep and 600 (i.e. 100 for each of the six) Medium Survey PSPC fields, including randomly distributed point sources (folded through the spectrum-weighted PSF) and Poissonian counting noise. The input sources have fluxes between 1×10^{-15} and 10^{-12} erg cm^{-2} s^{-1}, and are generated using the best-fitting number–flux differential distribution derived in Section 3.1 as input model. The background (including unresolved sources) was adjusted to match the level observed in the real survey fields. Each simulated field was searched for sources with PSS and its log N–log S distribution was constructed. The results of these simulations are shown in Fig. 3 for the Deep Survey and Fig. 4 for the Medium Survey.

The departure from the input model at low fluxes, where faint sources are not resolved from the general background, becomes significant below $\sim2.5\times10^{-15}$ and $\sim6\times10^{-15}$ erg cm^{-2} s^{-1} for the Deep and Medium Surveys, respectively. Examination of the 68 per cent confidence regions in Figs 3 and 4 leads us to conclude that the Deep Survey is essentially complete down to a limiting sensitivity of about 3×10^{-15} erg cm^{-2} s^{-1} and the individual Medium Survey fields are complete down to between 6 and 8×10^{-15} erg cm^{-2} s^{-1}. Clearly the use of the PSS routine is an effective method of selecting sources even at, and past, the formal confusion limit.

Above $\sim2.5\times10^{-14}$ erg cm^{-2} s^{-1} for the Deep Survey and $\sim6\times10^{-14}$ erg cm^{-2} s^{-1} for the Medium Survey (Figs 3 and 4), we are missing sources because of their low surface density combined with the limited survey area. It is also clear that the derived log N–log S distributions lie above the input ones over most of the flux range. The number–flux distributions of the simulated sources follow the input model closely, implying that the discrepancy does not arise in the simulation software, but must be inherent to the source detection process. The likely explanation is that source fluxes are over-estimated because of source confusion: two sources below the detection threshold may merge to produce a spurious

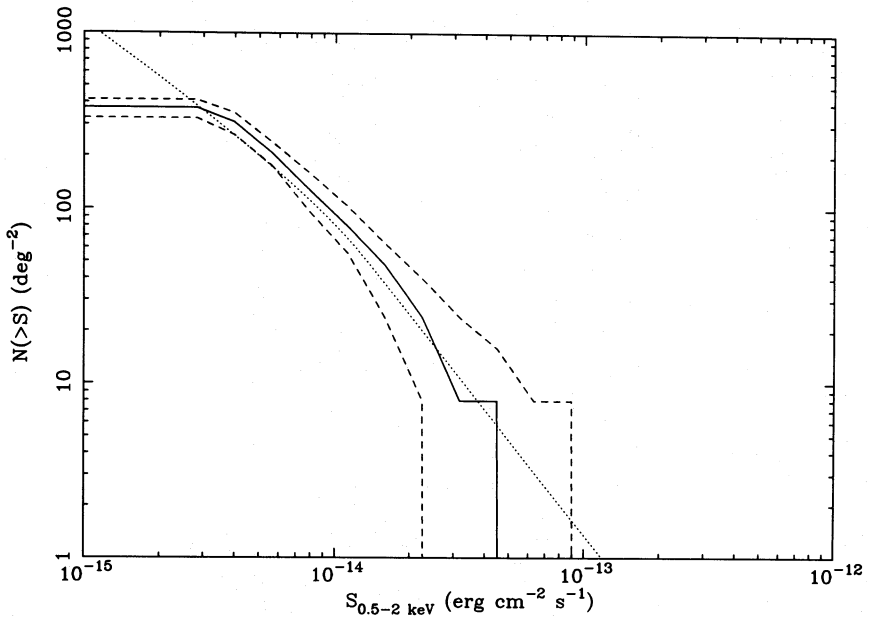

Figure 3. Results of point source detection simulations for the Deep Survey (see text for details). The median of the log N–log S relations obtained by running the PSS algorithm on 100 simulated PSPC images (solid line) is compared with the input model (dotted line). The dashed lines encompass the region where 68 per cent of the derived log N–log S relations fall.

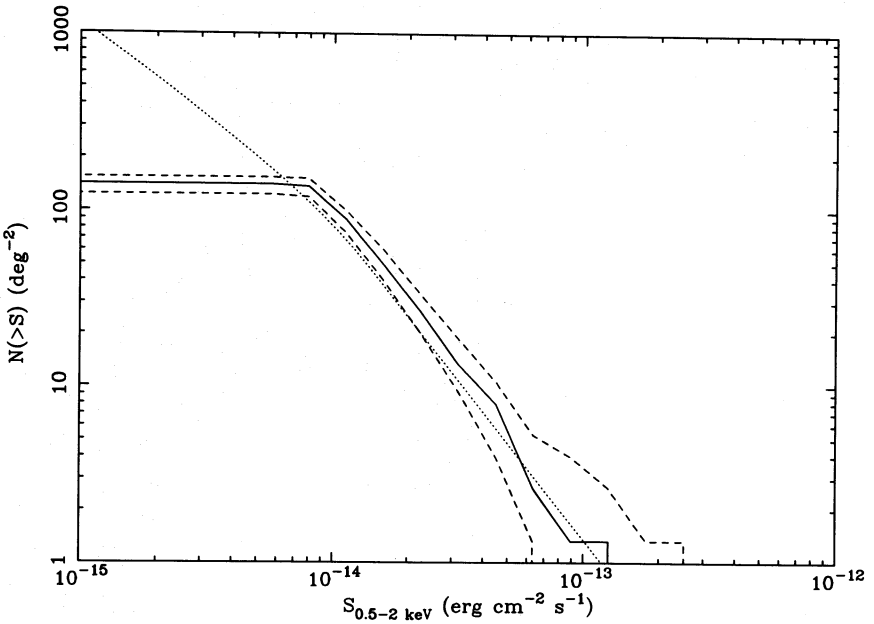

Figure 4. Results of point source detection simulations for the Medium Survey (see text for details). The median of the log N–log S relations obtained by running the PSS algorithm on 600 simulated PSPC images (solid line) is compared with the input model (dotted line). The dashed lines encompass the region where 68 per cent of the derived log N–log S relations fall.

detection, or two sources may be so close as to go unresolved spatially, and mimic a single, brighter detection. The net effect is an apparent increase in the number of sources detected, which is clearly most important at the faint flux end.

3.3 Derivation of the (corrected) log N–log S distribution

In the derivation of the cumulative number–flux distribution (log N–log S), we have made use of all sources detected in the Deep Survey up to a flux of 4×10^{-14} erg cm^{-2} s^{-1} (i.e. excluding the bright Galactic star; see Section 3), and those detected in the Medium Survey at or above a (conservative) flux of 8×10^{-15} erg cm^{-2} s^{-1}. We have again applied a ML technique and we have taken into account the results of the simulations (Section 3.2) as follows: each input model differential distribution has been multiplied by the fraction of input sources that have been detected in the simulations at any given flux, before comparing it with the observed distribution. The best-fitting model distribution has para-

meters (see Section 3.1 for definitions): $\gamma_1 = 1.78 \pm 0.38$, $\gamma_2 = 2.64 \pm^{1.19}_{0.52}$, $S_B = (1.64 \pm^{0.97}_{0.41}) \times 10^{-14}$ erg cm^{-2} s^{-1}, with $K = 72.9 \pm 28.3$ and $N(>10^{-14}) = 88.5$. The confidence intervals (90 per cent) were determined in the following way ('bootstrap' method). We simulated 1000 samples of 140 sources (i.e. as many as we detected, but excluding the Galactic star) by extracting them from the observed sample at random with reposition (i.e. a source might appear more than once in a simulated sample, and some sources might not appear at all). The ML technique was applied to each one of the simulated samples as described above, producing 1000 sets of best-fitting parameters. The quoted errors encompass 90 per cent of these bootstrap parameters. Our best-fitting model parameters agree, within the errors, with those determined by H93: $\gamma_1 = 1.94 \pm 0.19$, $\gamma_2 = 2.72 \pm 0.27$, $S_B = (2.66 \pm 0.66) \times 10^{-14}$ erg cm^{-2} s^{-1}, with $N(>10^{-14}) = 96.7$.

The (corrected) log N–log S distribution of the Deep and Medium Surveys is shown in Fig. 5, with the contribution of each source displayed (filled dots). The best-fitting model is indicated by the solid line. The distribution shows evidence for a smooth turn-over in the flux range between 1 and 2×10^{-14} erg cm^{-2} s^{-1}, and is inconsistent with a single power law of slope 2.5 (the Euclidean value) at $>3\sigma$. A flattening in the soft X-ray log N–log S distribution had originally been predicted from fluctuation analysis of *Einstein Observatory* Deep Survey fields (Hamilton & Helfand 1987; Barcons & Fabian 1990). Our result also confirms those of previous *ROSAT* observations (Hasinger, Schmidt & Trümper 1991; Shanks et al. 1991; H93).

4 CONTRIBUTION TO THE SOFT X-RAY BACKGROUND

We have used the detections made in the inner 12-arcmin radius of the Deep Survey field to estimate the contribution of discrete sources to the diffuse soft X-ray background directly. We first constructed the total spectrum (sources + background) by simply summing over this inner region. The background spectrum (diffuse + particle) was extracted by masking out all counts within 0.9 arcmin of the position of each source (93 per cent of flux encircled) and summing, except for the brightest source (the Galactic star in Section 3), for which we used a mask radius of 1.5 arcmin (95 per cent of flux encircled). The integrated source spectrum was derived by normalizing the background spectrum to the total area (0.13 deg^2) and subtracting it from the total spectrum. For the particle background we used the spectrum derived by Snowden et al. (1992), normalized to the total area. The particle contribution was then subtracted from the (diffuse + particle) background to produce the diffuse background spectrum.

Fig. 6 shows the diffuse background spectrum (solid line histogram) and the integrated spectrum of the sources detected within the inner 12-arcmin radius of the Deep Survey field, with and without including the Galactic star discussed in Section 3 (triangles and dots, top and bottom panels, respectively). The shape of the background spectrum is similar to that measured by Hasinger et al. (1991) in the North Ecliptic Pole (NEP) region, while our integrated source spectrum is much less cut off at low energies than that

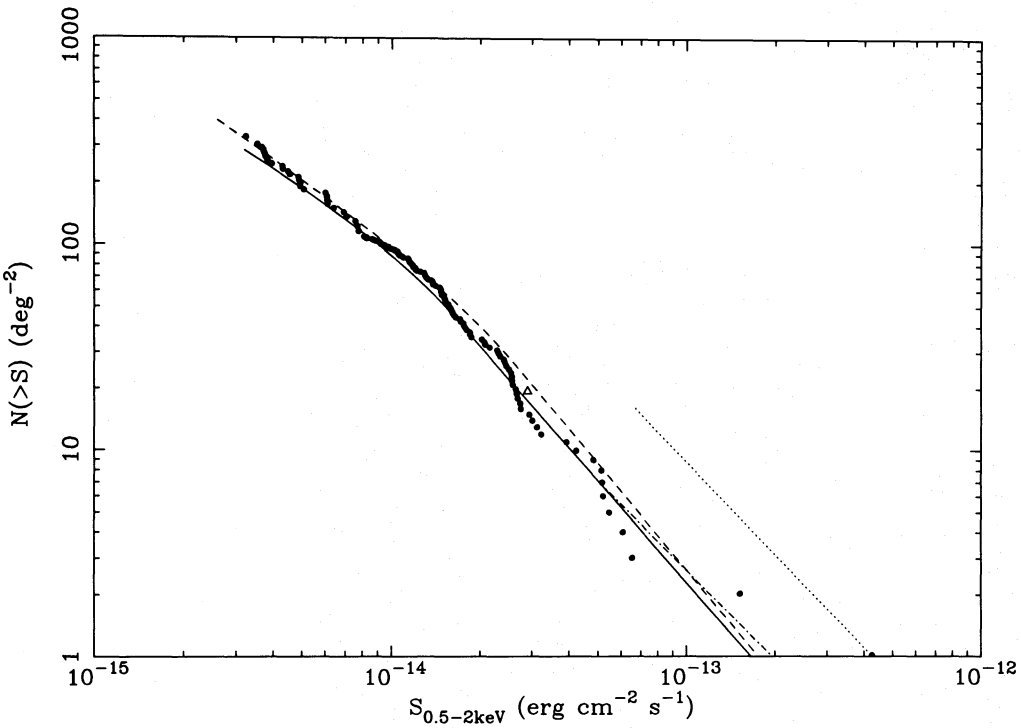

Figure 5. Cumulative number–flux distribution (log N–log S, 0.5–2.0 keV fluxes) of the sources detected in the Deep and Medium Survey fields (filled dots). Also plotted are the best fit to our data (solid line), the log N–log S approximation derived from the *ROSAT* survey of H93 (dashed line), the EMSS log N–log S relation (dot–dashed line) and that from the *Ginga* fluctuation analysis (dotted line) converted to the 0.5–2.0 keV band (see text for details), and the *Einstein* Deep Survey result (triangle).

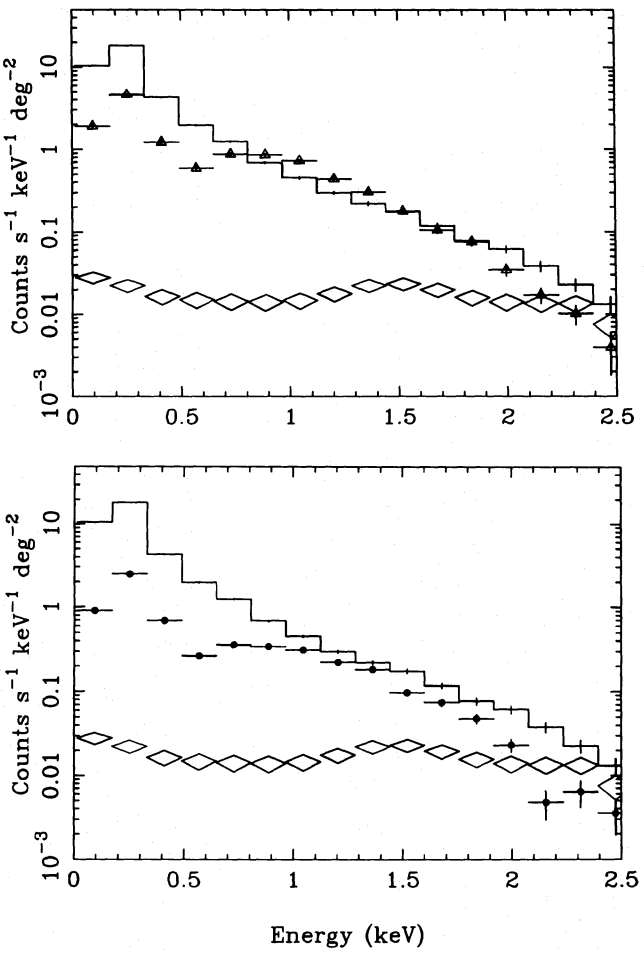

Figure 6. The spectrum of the diffuse soft X-ray background (solid line histograms) is compared with the integrated spectrum of the point sources detected in the Deep Survey field, with and without including the bright Galactic star (open triangles and filled dots, top and bottom panels, respectively; see text). In some cases the error bars are smaller than the sizes of the triangles and the dots. The particle background spectrum is indicated by the diamonds.

from the NEP region, reflecting the lower Galactic absorption column in our field. Our background spectrum appears flatter than that of the sources (excluding the Galactic star; lower panel in Fig. 6) in the energy range 1–2 keV. At lower energies there is a relative excess in the intensity of the background compared to the resolved sources, because of Galactic background emission and residual contamination by scattered solar X-rays. At and above 2 keV, uncertainties in the PSPC response and in the particle background flux preclude a meaningful comparison.

The integrated source spectrum is adequately fitted with a power-law model and low-energy absorption over the energy range 0.1–2.0 keV. There is no evidence for a 'soft excess' above the power-law fit at low energies: the minimum reduced χ^2 ($=1.6$, after attributing a 2 per cent systematic error to the flux in each spectral bin) does not decrease by including additional spectral components, such as a low-temperature blackbody or a thermal bremsstrahlung (the relatively high χ^2 probably reflects the synthetic nature of the spectrum). The best-fitting spectral slope is $\alpha = 1.16 \pm 0.11$ and the equivalent hydrogen column density $(7.6 \pm^{2.4}_{2.3}) \times 10^{19}$ cm^{-2} (90 per cent confidence errors). The latter is consistent with the column measured in the direction of the Deep Survey field (Section 2.1). The power-law slope agrees at 90 per cent confidence with that (0.96 ± 0.11, 0.1–2.0 keV) found by H93 for their sample of sources fainter than 4×10^{-14} erg cm^{-2} s^{-1} (which is also the flux of the brightest source detected in our Deep Survey and included in the integrated source spectrum), with the average energy index (0.9 ± 0.1, 0.5–2.0 keV) found by Wang & McCray (1993) for the sources detected in two deep images obtained with the *ROSAT* PSPC, and with the energy index (1.38 ± 0.25, 0.1–2.0 keV) measured with *ROSAT* by Turner, George & Mushotzky (1993) for a sample of bright Seyfert I galaxies.

The best representation of the diffuse background spectrum (again after including a 2 per cent systematic error) is obtained by fitting a multicomponent model, including a power law (to represent the extragalactic component), a Raymond–Smith plasma (as the Galactic contribution) and a Gaussian line at 0.54 keV (to account for the residual contamination by scattered solar X-rays; Snowden & Freyberg 1993). We fixed the equivalent hydrogen column absorbing the power law at 7.6×10^{19} cm^{-2} (see above). The fit requires a very cool Raymond–Smith plasma, with very little absorption, although the limited spectral resolution of the PSPC prevents us from determining the parameters of this component with precision; thus they were fixed at $N_{\rm H} = 4 \times 10^{18}$ cm^{-2} and $kT = 0.1$ keV in the fit, with solar values for the plasma elemental abundances. The best fit (reduced $\chi^2 = 1.8$) is obtained for a power-law energy slope of $0.71 \pm^{0.29}_{0.27}$ (90 per cent confidence). This is practically identical to the best-fitting index (0.72) found by Wang & McCray (1993) for the power-law component of the background in their two deep *ROSAT* images, and may indicate that sources below our detection limit on average possess a harder spectrum than those that are above it, in line with the hardness ratio results of H93. Wu et al. (1991), using several *Einstein Observatory* IPC fields at high Galactic latitude, also found a power-law component of slope ~ 0.7 in the spectrum of the cosmic X-ray background (0.5–3.5 keV).

The total intensity in the power-law component of the background, added to that of the sources actually detected in the Deep Survey field, but excluding the bright Galactic star, and before Galactic absorption, amounts to 2.7×10^{-8} erg cm^{-2} s^{-1} sr^{-1} (0.5–2.0 keV). The direct integration of the spectrum of the detected sources (1.2×10^{-8} erg cm^{-2} s^{-1} sr^{-1}) makes up 44 ± 4 per cent of this intensity (again ignoring the Galactic star; the error on the fraction includes the statistical uncertainty on the sources' flux and the errors on the parameters for the fit of the background). Repeating the calculation in the 1–2 keV range, we find a total intensity of $(1.4 \pm 0.1) \times 10^{-8}$ erg cm^{-2} s^{-1} sr^{-1} for the power-law component and the sources (which contribute 0.6×10^{-8} erg cm^{-2} s^{-1} sr^{-1}, i.e. 41 per cent of the total). This compares well with the extragalactic background intensity of 1.3×10^{-8} erg cm^{-2} s^{-1} sr^{-1} quoted by H93, considering the high uncertainties affecting measurements of this background. Using the *Einstein Observatory* IPC, Wu et al. (1991) found a total intensity (power-law component plus sources) of 5.6×10^{-8} erg cm^{-2} s^{-1} sr^{-1} (0.16–3.5 keV). Extrapolating our result to this energy band, we find a value of 5.8×10^{-8} erg cm^{-2} s^{-1} sr^{-1}, again in close agreement.

Integration of our source counts distribution from 3.2×10^{-15} erg cm^{-2} s^{-1} to infinity gives a total intensity which is the same as that of the sources detected in the Deep Survey field (1.2×10^{-8} erg cm^{-2} s^{-1} sr^{-1}, 0.5–2.0 keV). This is a satisfactory result, since our best-fitting log N–log S relation predicts that the contribution of sources brighter than those in the Deep Survey (i.e. above 5.6×10^{-13} erg cm^{-2} s^{-1}) is 6 per cent of the total above 3.2×10^{-15} erg cm^{-2} s^{-1}. (Using the *Einstein Observatory* EMSS log N–log S relation to extrapolate to infinite flux, the contribution above 5.6×10^{-13} erg cm^{-2} s^{-1} would be 12 per cent.) We can use the errors on the slope of our best-fitting log N–log S relation to calculate the upper and lower bounds on the fraction (44 per cent, see above) of the extragalactic X-ray background resolved into sources brighter than 3.2×10^{-15} erg cm^{-2} s^{-1}; they are 100 and 39 per cent, respectively (the errors on the slope of our log N–log S relation are used to compute errors on the resolved fractions throughout the following). The resolved fraction is $41\pm^{50}_{6}$ per cent in the 1–2 keV band, where H93 find that 59 per cent of the background is made up of discrete sources (with faintest limiting flux of 2.5×10^{-15} erg cm^{-2} s^{-1} in the 0.5–2.0 keV range). However, H93 use the source count distribution from the *Einstein Observatory* EMSS (Gioia, private communication), which includes Galactic and extragalactic contributions, to extrapolate to infinite flux.

5 DISCUSSION

5.1 Comparison with other log N–log S distributions

We have compared our log N–log S distribution with those from other *ROSAT* surveys, and from surveys carried out at higher energies. In addition to the best fit to our data (solid line), in Fig. 5 we plot the analytical approximation to the log N–log S distribution derived by H93 from their set of *ROSAT* observations (dashed line), and those from the *Einstein Observatory* EMSS (Gioia, private communication, and H93; dot–dashed line) and from *Ginga* fluctuation analysis (Warwick & Stewart 1989; dotted line). The triangle shows the source density determined in the *Einstein Observatory* Deep Survey (Primini et al. 1991), which is in good agreement with our results. Hamilton et al. (1991) also measured a very similar source density at this flux level in their log N–log S relation, derived from a reanalysis of the *Einstein Observatory* Deep Survey.

Comparison of our survey with that of H93 is straightforward because the same instrument was used in both cases. H93 adopt a count rate to flux conversion factor appropriate to a power law of energy index $\alpha=1$, while we use $\alpha=1.1$ (Section 2.2). Since our conversion factor is identical to H93, within 1 per cent, we have plotted the H93 best fit in Fig. 5 without correction. The log N–log S relation from the H93 survey lies above our best fit by as much as ~20 per cent, although we detect 95 sources per deg^2 above 10^{-14} erg cm^{-2} s^{-1}, while the H93 best fit gives 97 (our best fit gives 89).

The EMSS distribution also lies above our Deep and Medium Surveys at fluxes higher than 5×10^{-14} erg cm^{-2} s^{-1}. Preliminary optical identification work suggests that the Galactic contamination of our sample is only about 10 per cent, while the Galactic stellar content of the EMSS is ~25 per cent (Stocke et al. 1991), but this explains only part of the discrepancy. Gioia used a power-law spectrum of energy slope $\alpha=1$ to convert from IPC count rates to 0.3–3.5 keV fluxes, and a value of Galactic absorption appropriate to each one of her fields; the use of $\alpha=1.1$ (as we do) would lead to a maximum of ~4 per cent difference in the 0.5–2.0 keV fluxes, which we have not corrected for in the plot.

The conversion between *Ginga* (2–10 keV) and *ROSAT* (0.5–2.0 keV) fluxes is more uncertain. The simplest approach is to assume that the *Ginga* background fluctuations are produced by the same population of active galactic nuclei (AGN) that are resolved by *ROSAT*. The spectrum of the *Ginga* fluctuations has an energy slope of 0.7 (Warwick & Stewart 1989), while in the *ROSAT* band we observe a mean slope of 1.16 for the resolved sources. As an example, we have adopted a broken power-law spectrum with a break at 2 keV, and energy slopes of 0.7 and 1.2 above and below the break, respectively. The *Ginga* extrapolation (dotted line in Fig. 5) disagrees with our Deep and Medium Survey log N–log S relation by a factor of about 4. A similar result was found by Warwick & Stewart (1989), when comparing the extrapolation of the *Ginga* source counts distribution with the *Einstein Observatory* EMSS. We conclude, as they did, that only a much flatter spectral slope below 2 keV would reconcile the *Ginga* and *ROSAT* distributions. A more realistic explanation, already put forward by Warwick & Stewart, is that most of the sources seen in the *Ginga* range may be too absorbed to contribute substantially in the *ROSAT* band.

5.2 Resolving the X-ray background

Our Deep and Medium Surveys with the *ROSAT* PSPC allow us to construct a source number–flux distribution (log N–log S) in the soft X-ray band (0.5–2.0 keV) which extends to fluxes that are an order of magnitude fainter than was possible before the advent of *ROSAT* and which is the second deepest published so far (the deepest being that of H93, with a limiting sensitivity for source detection of 2.5×10^{-15} erg cm^{-2} s^{-1} in the 0.5–2.0 keV band). Thus we are in a position to make accurate statements and predictions on the amount of soft X-ray background resolved into discrete sources. Surveys in the soft X-ray band to very faint limiting fluxes are still rare, because of the large amounts of telescope time they require; this makes the comparison of our results with those of H93 especially important.

By comparing the integrated spectrum of the sources in the Deep Survey field with the extragalactic power-law component of the diffuse X-ray background, we have determined that 44 ± 4 per cent of it is directly resolved (0.5–2.0 keV). By integrating our best-fitting log N–log S distribution to infinite flux, we estimate that sources above a flux of 3.2×10^{-15} erg cm^{-2} s^{-1} contribute $44\pm^{56}_{5}$ per cent of the background intensity. Extrapolating our fit to zero flux, and integrating, we resolve $89\pm^{11}_{33}$ per cent of the background.

It is possible to explore the behaviour of the log N–log S distribution at fainter flux levels than is allowed by individual source detection by examining background fluctuations, via the so-called $P(D)$ analysis. The results of applying this technique to our *ROSAT* Deep and Medium Surveys have been reported by Barcons et al. (1994, hereafter B94). In brief, the log N–log S relation is found to extend with a flat

slope (1.8) to at least a flux of 7×10^{-16} erg cm^{-2} s^{-1}, with between 900 and 1800 sources per deg^2 expected at or above this flux level. If the log N–log S plot turns up at low fluxes, this must happen below the flux limit reached by the $P(D)$ analysis.

Extrapolating and integrating our log N–log S best fit down to the $P(D)$ flux limit of 7×10^{-16} erg cm^{-2} s^{-1}, we find that $56\pm^{44}_{8}$ per cent of the background is resolved, in good agreement with B94 (60 per cent resolved); using our 90 per cent confidence upper bound for the slope γ_1 (2.16), we exceed the background, as do B94 for their upper bound slope of 2.0. In order to increase the resolved fraction to 100 per cent at zero flux, the flattest slope we require below 7×10^{-16} erg cm^{-2} s^{-1} is 1.83, well within our confidence limits and those of B94. Similarly, H93, using a slope of 1.94 to represent their log N–log S relation at the faint flux end, and the results of their fluctuation analysis, are able to resolve the whole background in the 1–2 keV band by extrapolating to zero flux. If a Euclidean component is present below our $P(D)$ flux limit, we find that the background is saturated at 4.3×10^{-17} erg cm^{-2} s^{-1}, with a source density of $\sim4\times10^4$ source per deg^2.

A detailed discussion of the origin of the flattening in the source counts distribution is beyond the scope of this paper. The results of the $P(D)$ analysis of the Deep Survey field, which allows us to extend our log N–log S relation to fainter fluxes, and their implications on the population of sources contributing to the extragalactic soft X-ray background have been discussed by B94. In summary, while the flattening in the source counts distribution at $\sim2\times10^{-14}$ erg cm^{-2} s^{-1} can be explained by the diminishing contribution of emission-line AGN whose luminosities are evolving with time (Maccacaro et al. 1991; Boyle et al. 1993), a re-steepening at fluxes below the $P(D)$ analysis limit would require the presence of a new population of sources, for instance starburst galaxies and low-luminosity AGN, or a population of sources with an absorbed X-ray spectrum.

6 CONCLUSIONS

Our principal results are as follows.

(i) Our source counts differential distribution in the 0.5–2.0 keV range has a best-fitting slope of 2.6 above $\sim2\times10^{-14}$ erg cm^{-2} s^{-1} and 1.8 below this flux level. Thus we confirm the flattening of the distribution previously found in the *ROSAT* surveys of Shanks et al. (1991), Hasinger et al. (1991) and H93. Moreover, the good agreement, in shape and normalization, with the distribution obtained by H93 from the only *ROSAT* survey deeper than ours, is particularly significant because it is the product of totally independent determinations of the source counts distribution at faint fluxes, using different source selection criteria and different data analysis techniques.

(ii) The direct integration of the spectrum of the sources detected in the central 12-arcmin radius of the Deep Survey field makes up 44 ± 4 per cent of the total 0.5–2.0 keV extragalactic background, which we have estimated by adding the sources' contribution to that of the power-law component of the observed diffuse background. Integrating our best-fitting log N–log S distribution above 3.2×10^{-15} erg cm^{-2} s^{-1}, and using the 90 per cent errors on its parameters, we calculate a background resolved fraction of $44\pm^{56}_{5}$ per cent. The $P(D)$ analysis of the Medium and Deep Survey fields reported by Barcons et al. (B94) shows that the slope of the number–flux relation maintains a value of 1.8 down to a flux of 7×10^{-16} erg cm^{-2} s^{-1}, and that a re-steepening, if it is necessary to resolve the whole extragalactic X-ray background, can only take place at lower fluxes.

(iii) The integrated spectrum of the sources in the Deep Survey field is satisfactorily fitted with a single power law, and an amount of low-energy absorption consistent with the Galactic neutral hydrogen column. The source spectrum is steeper ($\alpha=1.16$) than the power-law component ($\alpha=0.71$) fitted to the background. This is in line with the hardness ratio results of H93, which show that fainter sources tend to possess harder X-ray spectra.

ACKNOWLEDGMENTS

KOM, ACF and RGM acknowledge the support of the Royal Society. We thank the referee for constructive comments and suggestions.

REFERENCES

Allan D. J., Ponman T. J., 1991, ASTERIX Data Analysis, Application Note 001
Barcons X., Fabian A. C., 1990, MNRAS, 243, 366
Barcons X., Branduardi-Raymont G., Warwick R. S., Fabian A. C., Mason K. O., McHardy I., Rowan-Robinson M., 1994, MNRAS, 268, 833 (B94)
Boulanger F., Pérault M., 1988, ApJ, 330, 964
Boyle B. J., Griffiths R. E., Shanks T., Stewart G. C., Georgantopoulos I., 1993, MNRAS, 260, 49
Cash W., 1979, ApJ, 228, 939
Condon J. J., 1974, ApJ, 188, 279
Eddington A. S., 1940, MNRAS, 100, 354
Gioia I. M., Maccacaro T., Schild R. E., Stocke J. T., Liebert J. W., Danziger I. J., Kunth D., Lub J., 1984, ApJ, 283, 495
Gioia I. M., Maccacaro T., Schild R. E., Wolter A., Stocke J. T., Morris S. L., Henry J. P., 1990, ApJS, 72, 567
Hamilton T. T., Helfand D. J., 1987, ApJ, 318, 93
Hamilton T. T., Helfand D. J., Wu X., 1991, ApJ, 379, 576
Hasinger G., Schmidt M., Trümper J., 1991, A&A, 246, L2
Hasinger G., Turner T. J., George I. M., Boess G., 1992, Legacy, 2, 77
Hasinger G., Burg R., Giacconi R., Hartner G., Schmidt M., Trumper J., Zamorani G., 1993, A&A, 275, 1 (H93)
Jones M. H., Rowan-Robinson M., Branduardi-Raymont G., Smith P., Pedlar A., Willacy K., 1994, MNRAS, submitted
Lockman F. J., Jahoda K., McCammon D., 1986, ApJ, 302, 432
Maccacaro T. et al., 1982, ApJ, 253, 504
Maccacaro T., Romaine S., Schmitt J. H. M. M., 1987, in Hewitt A., Burbidge G., Fang L. Z., eds, Proc. IAU Symp. 124, Observational Cosmology. Reidel, Dordrecht, p. 597
Maccacaro T., Della Ceca R., Gioia I. M., Morris S. L., Stocke J. T., Wolter A., 1991, ApJ, 374, 117
Primini F. A., Murray S. S., Huchra J., Schild R., Burg R., Giacconi R., 1991, ApJ, 374, 440
Rowan-Robinson M., Hughes J., Jones M., Leech K., Vedi K., Walker D. W., 1991, MNRAS, 249, 729
Schmitt J. H. M. M., Maccacaro T., 1986, ApJ, 310, 334
Shanks T., Georgantopoulos I., Stewart G. C., Pounds K. A., Boyle B. J., Griffiths R. E., 1991, Nat, 353, 315
Snowden S. L., Freyberg M. J., 1993, ApJ, 404, 403

Snowden S. L., Plucinsky P. P., Briel U., Hasinger G., Pfeffermann E., 1992, ApJ, 393, 819
Stark A. A., Gammie C. F., Wilson R. F., Ball J., Linke R. A., Heiles C., Hurwitz M., 1992, ApJS, 79, 77
Stocke J. T., Morris S. L., Gioia I. M., Maccacaro T., Schild R., Wolter A., Fleming T. A., Henri J. P., 1991, ApJS, 76, 813
Turner T. J., George I. M., Mushotzky R. F., 1993, ApJ, 412, 72
Wang Q. D., McCray R., 1993, ApJ, 409, L37
Warwick R. S., Stewart G. C., 1989, ESA SP-296, 2, 727
Wu X., Hamilton T., Helfand D. J., Wang Q., 1991, ApJ, 379, 564